NANO LETTERS

2006
Vol. 6, No. 9
2037−2042

Surface Plasmons and Vibrations of Self-Assembled Silver Nanocolumns

Jeremie Margueritat*

Laser Processing Group, Instituto de Optica, CSIC, Serrano 121, 28006 Madrid, Spain, and Laboratoire de Physique des solides, UMR 5477 CNRS, Université Paul Sabatier, 118 route de Narbonne, 31062 Toulouse Cedex 4, France

Jose Gonzalo and Carmen N. Afonso

Laser Processing Group, Instituto de Optica, CSIC, Serrano 121, 28006 Madrid, Spain

Adnen Mlayah

Laboratoire de Physique des solides, UMR 5477 CNRS, Université Paul Sabatier, 118 route de Narbonne, 31062 Toulouse Cedex 4, France

Daniel B. Murray

Mathematics, Statistics and Physics Unit, University of British Columbia Okanagan, 3333 University Way, Kelowna, British Columbia, Canada V1V 1V7

Lucien Saviot

Laboratoire de Recherche sur la Réactivité des Solides, UMR 5613 CNRS, Université de Bourgogne, 9 avenue A. Savary, BP 47870-21078 Dijon, France

Received May 31, 2006; Revised Manuscript Received August 1, 2006

ABSTRACT

Optical and vibrational properties of novel self-assembled silver nanocolumns are studied experimentally and theoretically. The split of the surface plasmon resonance into transverse and longitudinal modes verifies the one-dimensional character of the nanocolumns. In this work, we have identified the acoustic vibration modes of the nanocolumns using Raman scattering, as spheroid-like modes ($l = 2$, $m = \pm 2$) involving vibrations of the nanocolumns along their minor axes and the existence of surface plasmon-vibration coupling mechanisms.

Recently, there has been great interest in the optical properties of metal nanoparticles (NPs). Much of this interest is stimulated by the possibility of generating large electromagnetic field enhancement via surface plasmon resonance (SPR) in different types of optical spectroscopies (Raman, Brillouin, and Rayleigh scattering, linear absorption).[1−5] Moreover, metal NPs exhibit unique size- and shape-dependent SPR, which make them ideal candidates for the design of new electronic and optical devices.[6−8] Thus, the control of the size and shape of structures at the nanoscopic level is now one of the most challenging issues faced by physicists and chemists working in nanoscience.

Several methods have been developed to produce elongated metal NPs and nanorods such as electrochemical techniques,[8] templates (i.e., mesoporous silica,[9] alumina,[3−4] or carbon nanotubes[10]), polymer-directed synthesis and sandwich reduction processes.[11−15] Thin-film technologies are particularly suited for the production of embedded metallic nanorods. Among them, alternate pulsed laser deposition has proved its potential for the production of embedded metallic NPs with reduced size dispersion,[16] and recently it has been used to successfully grow self-assembled oriented silver nanocolumns (NCls) embedded in amorphous Al_2O_3.[17]

In this letter, we report on the effect of the elongated shape of the NCls along the growth direction on their optical and vibrational properties using linear absorption spectroscopy and Raman scattering. Because the surface plasmons might play the role of intermediate states in the inelastic light-scattering process under resonant optical excitation, and thus trigger the emission and absorption of vibration modes, we

* Corresponding author. E-mail: j.margueritat@io.cfmac.csic.es.

10.1021/nl061237h CCC: $33.50
Published on Web 08/22/2006

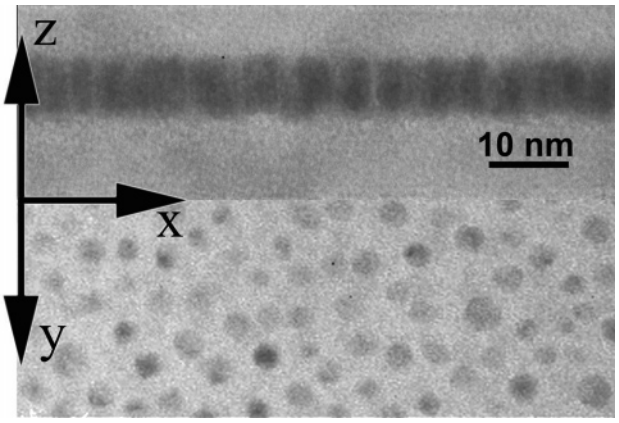

Figure 1. Cross-section (z) and plan-view (x,y) images of the specimen containing self-assembled silver NCls embedded in a-Al_2O_3. (x,y) is the substrate plane.

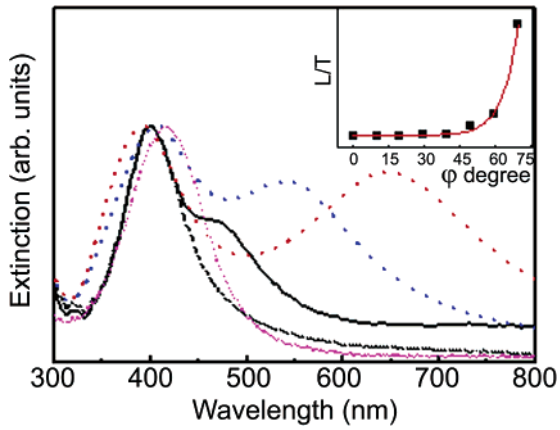

Figure 2. Extinction spectra of silver NCls and NPs. Black curves are experimental spectra of NCls recorded with p- (continuous line) and s-polarized light (dotted line). The violet curve is the experimental spectrum of NPs recorded with nonpolarized light. Red and blue curves, respectively, show the spectra of NCls simulated using Gans and Maxwell−Garnett models. The inset shows the experimental longitudinal (L) to transverse (T) intensity ratio of the SPR modes versus the angle of incidence (φ) when using p-polarized light.

investigate the shape and polarization dependences of the Raman scattering excited at wavelengths close to SPR. Two main advantageous features of the NCls for the study of this interaction can be stressed. First, all NCls are oriented in the same direction, which opens the possibility for studying anisotropy effects. Second, the small dispersion both in diameter and height reduces the inhomogeneous broadening of the optical transitions considerably.

The samples studied in this work were produced by pulsed laser deposition using an ArF excimer laser (pulse duration 20 ns, energy density 1.9 J.cm^{-2}). The beam was alternately focused on the surface of high purity Al_2O_3 and Ag rotating targets. The NCls have been produced by growing five layers of silver NPs embedded in a-Al_2O_3 with average diameter $\boldsymbol{D}_{\mathrm{NP}} = 2.0 \pm 0.2$ nm. Reducing the layer-to-layer distance down to $\boldsymbol{D}_{\mathrm{NP}}$, the NPs of consecutive planes get in contact, inducing the vertical self-assembling of the NPs due to coalescence. They eventually form NCls as seen in the cross-section and plan-view images obtained by transmission electron microscopy (TEM) shown in Figure 1.[17] The average height of the NCls is $\boldsymbol{H} = 6.7 \pm 0.2$ nm, and their average diameter is $\boldsymbol{D}_{\mathrm{NCl}} = 2.7 \pm 0.2$ nm. Thus, the aspect ratio is $\boldsymbol{H}/\boldsymbol{D}_{\mathrm{NCl}} = 2.5 \pm 0.3$. The number density of the NCls is $(7.8 \pm 0.2) \times 10^{12}$ cm^{-2}, which corresponds to 3.6 nm (center to center) average separation. Although the deposition technique allows excellent control of the average NCl or NP diameter, similar control over the number density of NPs in the layer and thus over the average coverage or filling factor cannot be achieved. The random character of the nucleation process on the a-Al_2O_3 surface makes diameter and coverage-related parameters. Further details of the production procedure and NCl morphology can be found in an earlier work,[17] where it was also shown that the NCls are polycrystalline. The specimens were grown simultaneously on glass and silicon substrates in order to perform optical transmission measurements and Raman measurements on the same specimens, while avoiding the use of glass substrates in the latter case, because this would have provided a background signal in the low-frequency range.

The extinction spectra, calculated as $-\ln T$ of the transmission spectra, were recorded using a WVASEJA Woollman ellipsometer. The light beam was either p- or s-polarized, and the angle of incidence was 65° with respect to the normal to the surface. Because of the high refractive index of a-Al_2O_3, the beam propagates inside the layer at only 33°. The investigated spectral range was 300−800 nm, and the spectral resolution was $\Delta\lambda = 3.5$ nm. The measurements were corrected for the background spectral response of the glass substrate.

In the near UV−visible range, the extinction spectrum of silver NPs is dominated by the SPR[16,18−22] whose wavelength depends mainly on size and shape of absorbing/scattering objects. In the case of five well-separated layers of spherical NPs with average diameters of 2.0 ± 0.2 nm embedded in a-Al_2O_3,[17] the SPR appears as a single band located around 415 nm (Figure 2) and no dependence on the incident light polarization is observed. As the NPs are distorted and become prolate or oblate, this band splits into longitudinal and transverse SPR modes corresponding to dipole oscillations along the major and minor axes, respectively. Such a splitting is observed in the extinction spectrum of Ag NCls recorded with p-polarized light (shown in Figure 2). In this case, the incident electric field excites both the longitudinal and transverse SPR at 470 and 400 nm that are along the major and minor axis of the NCls, respectively. Instead, only dipole oscillations along the minor axis of the NCls could be excited with s-polarized light and thus the extinction spectrum only shows the transverse SPR mode at 400 nm. The inset in Figure 2 shows the variation of the intensity of the longitudinal to transverse modes ratio as a function of the angle of incidence using p-polarized light. The intensity of the longitudinal mode strongly increases for grazing incidence, confirming that the longitudinal polarization vector is excited when the incident electric field is aligned along the major axis of the NCls.

Optical extinction spectra have been simulated in order to correlate the measured SPR wavelengths to the aspect ratio

H/D_{NCl} of the NCls. We have assumed that the NCls have a prolate spheroidal shape, rather than a rod-like shape. Because the NCls are polycrystalline, we have used the bulk silver frequency-dependent dielectric function for the NCls,[23] although corrected for the size- and shape-induced homogeneous broadening of the plasmon excitations.[18,19,24] A dielectric constant $\epsilon_m = 2.79$ was used for the a-Al_2O_3.[25]

We first considered the model proposed by Gans,[21,26] which is an extension of Mie's theory to spheroidal NPs. The simulated spectrum is included in Figure 2 and predicts a longitudinal SPR at 650 nm, that is, red-shifted by 180 nm with respect to the experimental value. The theory[23,24] also predicts that the longitudinal to transverse SPR splitting increases as the aspect ratio is increased. This has been observed experimentally by several authors.[18−21] The differences between the Gans model and the experimental results in Figure 2 could be related to the high number density of NCls ($(7.8 \pm 0.2) \times 10^{12}$ cm^{-2}). To clarify this point, we have also considered the Maxwell−Garnett effective medium model adapted to prolate particles.[27,28] In addition to the size and aspect ratio, this model takes into account the volume fraction, f, occupied by the NCls that is estimated to be $f = 0.3$ from TEM images shown in Figure 1. The extinction spectrum calculated using the Maxwell−Garnett model is also shown in Figure 2. The longitudinal SPR now appears at 540 nm, whereas the transverse SPR is at 407 nm, both closer to experimental values than the ones achieved with the Gans model. The main effect of taking into account the local field correction due to the effective medium surrounding the particle is the partial screening of the longitudinal SPR. This reduces the longitudinal to transverse wavelength splitting with respect to the case of isolated spheroidal NPs in the Gans model. In spite of the fact that both models predict the splitting of SPR related to the elongated shape of the NCls, both provide a longitudinal to transverse SPR splitting larger than the experimental one. The discrepancies between simulations and experiments are most likely related to the assumptions used in the models such as prolate NPs (NCls shape does not completely match this shape) or dilute system ($f << 1$ instead of $f = 0.3$ in our system).

Low-frequency Raman measurements were performed on a T800 Coderg spectrometer using different Argon and Krypton laser lines ranging from 413 to 514 nm. The incident beam was either p- or s-polarized, and the angle of incidence was 60° with respect to the normal to the sample surface. The scattered light was detected along the normal to the surface and was the same for p and s polarizations. Figure 3 shows Stokes and anti-Stokes low-frequency Raman spectra of the sample containing NCls excited with p polarization at 488 nm. For comparison, we also show the spectrum recorded from the sample containing spherical NPs. The band observed at 26 ± 2 cm^{-1}, which is a characteristic feature of spherical metal NPs,[29−31] is due to scattering by quadrupolar acoustic vibration modes ($l = 2$). As shown already,[32] these modes are Raman active because of their strong interaction with the dipolar SPR associated with the modulation of the surface polarization charges (surface orientation mechanism). Moreover, according to Lamb's

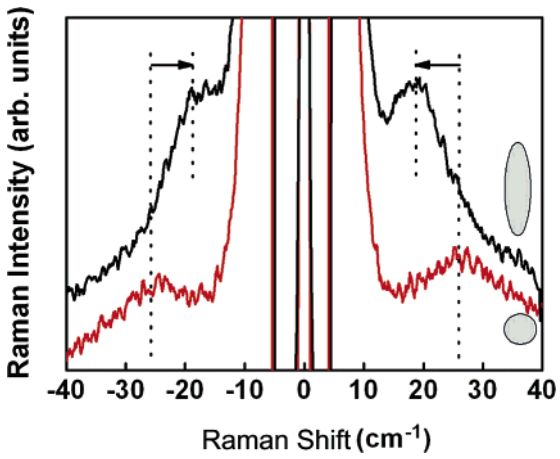

Figure 3. Stokes and anti-Stokes room-temperature Raman spectra of Ag NCls (black line) and spherical NPs (red line) excited at 488 nm. The incident laser beam was p-polarized, and the polarization of the scattered intensity was not analyzed. Dotted vertical lines and arrows highlight the shift of the Raman bands of the NCls with respect to those of spherical NPs.

model,[33] the vibration frequencies of quadrupolar acoustic modes of a free spherical NP are inversely proportional to their size. The fundamental frequency is given by[34,35] $\omega = 0.85 v_t/(cD_{NP})$, where v_t is the transverse sound velocity of bulk Ag and c is the vacuum light velocity. Using the experimental value, $\omega_{exp} = 26 \pm 2$ cm^{-1} for spherical NPs and $v_t = 1660$ ms^{-1},[36] one obtains a diameter of 1.80 ± 0.15 nm that is in good agreement with the experimental value ($D_{NP} = 2.0 \pm 0.2$ nm) obtained by TEM.

The Raman signal associated with acoustic vibrations of the NCls is shifted to lower frequencies by 7 cm^{-1} with respect to that of the spherical NPs (Figure 3), while its intensity is approximately 4 times higher than that of spherical NPs. These differences are a consequence of the excitation wavelength (488 nm) being nearly resonant with the longitudinal SPR mode as seen in Figure 4, which shows the extinction spectra of NCls together with the frequency of Raman bands as a function of excitation wavelength. The incident beam was always p-polarized, and the polarization of scattered light was not analyzed. A blue shift (4 cm^{-1}) of the Raman band is observed when getting close to the SPR with the longitudinal SPR (from a to d). Similar observations were reported already[36] for spherical NPs and were related to both inhomogeneous broadening of the Raman band and different size dependence of the resonant and non-resonant Raman scattering efficiencies mediated by SPR.[32] When using the 413 nm line (e), the optical excitation is close to the transverse SPR and, consequently, the Raman peak is shifted to a significantly lower frequency (20 cm^{-1}). This is consistent with a different vibration mode involved in the plasmon-vibration coupling mechanism.

To investigate the interactions between SPR modes and confined acoustic vibrations further, we have recorded Raman spectra for various incident and scattered polarization angles. Figure 5 shows that the Raman signal is observed only when the incident light is p-polarized irrespective of the polarization of the scattered light. The inset in Figure 5 shows the evolution of the Raman intensity as a function of

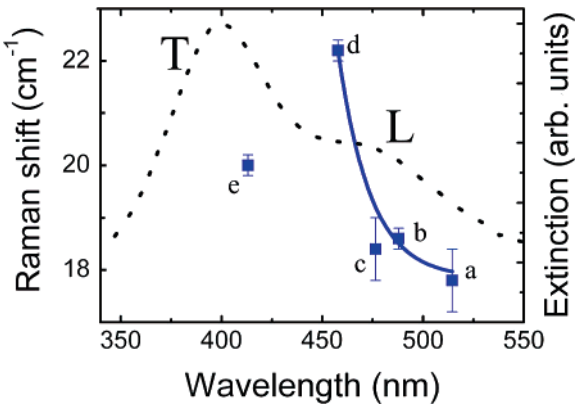

Figure 4. Filled squares (left scale): experimental frequencies of the NCl's vibrations versus excitation wavelength: (a) 514.5 nm; (b) 488 nm; (c) 476.5 nm; (d) 457.9 nm; and (e) 413.1 nm. The laser beam was always p-polarized, and the scattered light was not analyzed. The full line is a guide to the eye. The p-polarized extinction spectrum of the NCls (discontinuous line, right scale) is shown to ease the location of the excitation lines with respect to the SPR (T and L stand for transverse (x,y) and longitudinal (z) modes).

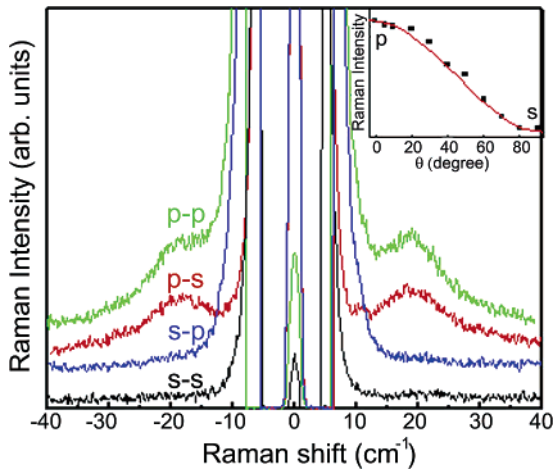

Figure 5. Raman spectra of NCls excited at 488 nm and using different polarizations. "A−B" stands for (A) incident and (B) scattered polarizations, respectively. The inset shows the intensity variation of the low-frequency Raman band versus excitation polarization angle (from p to s) normalized with respect to that of the optical phonon of silicon. The continuous line is an empirical $\cos^2(\theta)$ fit.

the incident polarization angle from p (0°) to s (90°). The measured intensity has been normalized to that of the optical phonon of the silicon substrate, that is, to the number of photons that have penetrated the sample. In that way, the Raman intensity changes are only due to the different excitation conditions. The scattered intensity is found to vary as $\cos^2(\theta)$ (where θ is the incident polarization angle), which indicates that it is maximum when the incident polarization component is along the major axis (z) of the NCls, that is, the longitudinal SPR becomes excited. This is a clear effect of the elongated shape and self-alignment of the scattering objects along the z axis. However, the electric field producing the photons detected in our experimental conditions is always along the perpendicular to the major axis of the NCls ((x,y) plane), that is, parallel to transverse surface plasmons.

Table 1. Measured Frequencies (ω_{exp}) of the Raman Bands and Calculated Frequencies (ω_{MD}) of the Confined Acoustic Vibrations of Spherical NPs and NCls[a]

	NP modes	NCl modes	
ω_{exp} (cm^{-1})	26 ± 2		19.2 ± 2
ω_{MD} (cm^{-1})	23.4	9.6	17.1
ω_{corr}(cm^{-1})	25.9	12.1	19.6
assigned vibrational modes	$l = 2$, $m = 0, \pm1, \pm2$ $S = 0.85$	$l = 2$, $m = 0, \pm1$ $S = 0.44$	$l = 2$, $m = \pm2$ $S = 0.8$

[a] The latter were obtained by molecular dynamic simulations. ω_{corr} includes an additive correction of 2.5 cm^{-1} over ω_{MD} to account for the effect of the surrounding medium.

Because the NCls have symmetry of revolution around the z axis, the scattered intensity should be the same in both p−p and p−s configurations as observed experimentally in Figure 5. This dependence of the Raman scattered intensity on the incident and scattered polarizations allows us to conclude that surface plasmon excitations indeed act as intermediate (collective) electronic states in the light-scattering process. This reasoning is thus consistent with the polarization vector associated with the longitudinal SPR mode being modulated by the NCl's vibrations. As a result of this interaction, the transverse SPR mode becomes excited and contributes to the recorded Raman response. The fact that the photon emission step is not resonant because the transverse SPR is located at 400 nm, whereas the wavelength of the scattered photons is very close to the excitation line (488 nm), as shown in Figure 4, further supports the coupling of the longitudinal SPR mode to acoustic vibrations, causing Raman scattering.

To identify the acoustic vibration modes responsible for the measured Raman signal, we have performed molecular dynamic (MD) simulations.[37] Because the elastic properties of monocrystalline silver are strongly dependent on crystallographic direction,[36] and in the present case the NCls are polycrystalline,[17] we have assumed isotropic elasticity and we used sound velocities $v_L = 3750$ m/s and $v_T = 1740$ m/s obtained by averaging the elastic constants of silver over all directions. We also assumed that the NCls have a prolate spheroidal shape and are free-standing; that is, the a-Al_2O_3 host has no influence on the vibrations. The calculated frequencies of quadrupolar vibration modes (ω_{MD}) of free-standing spherical particles are summarized in Table 1. This frequency is shifted with respect to the experimental one by 2.5 cm^{-1}, which can be attributed to the matrix-induced frequency shift. This shift will be used in the following to take into account the effect of the matrix and thus obtain ω_{corr} values.

The simulations predict that the fivefold degenerate quadrupolar vibration modes $l = 2$, initially at the dimensionless frequency $S = \omega(c\boldsymbol{D})/v_t = 0.85$, splits into three different frequencies when the aspect ratio becomes higher than 1. For an aspect ratio $\boldsymbol{H}/\boldsymbol{D}_{NCl} = 2.5 \pm 0.3$ two of these frequencies are close to each other: the ($l = 2$, $m = 0$) and ($l = 2$, $m = \pm1$) modes that occur around $S = 0.44$. The third frequency is close to $S = 0.8$ and is associated with

the ($l = 2$, $m = \pm 2$) modes. The corresponding frequencies ω_{MD} are given by $S v_t/(c\boldsymbol{D}_{NCl})$ and are listed in Table 1. We will refer to these modes as spheroidal-like modes (SLMs) because they are truly spheroidal modes (SMs) only for a perfect sphere.

Under resonant excitation, the frequency of the Raman band of the NCls is very close to the calculated frequency of the SLMs ($l = 2$, $m = \pm 2$) that involve vibrations along the minor axes only. For SLMs ($l = 2$, $m = +2$), the particle contracts along the x axis while elongating along the y axis and being unchanged along the major axis (z). There is good agreement between the calculated frequencies of the SLMs ($l = 2$, $m = \pm 2$) and measured frequencies, but the coupling mechanism between the vibrational modes and the SPR modes needs to be specified. According to the experimentally observed Raman selection rules for our scattering configuration (Figure 5), the active vibrational modes should lead to some polarization transfer from the longitudinal (excited) to the transverse surface plasmons (detected). In other words, the longitudinal polarization should be projected along the transverse directions (x and y) by the SLMs. The SMs ($l = 2$, $m = \pm 2$) are not expected to produce such a projection because they produce no modulation along the major axis of the NCls. However, as mentioned above, the NCl's modes are not truly spheroidal and they might also involve modulation along the z axis, which should lead to a detectable modulation of the polarization associated with the longitudinal SPR. Moreover, deviations from the perfect prolate shape (i.e., rod-like shape), should affect the SPR and also the vibrational eigenvectors, thus possibly leading to modulation of the longitudinal polarization.

The SLMs ($l = 2$, $m = 0, \pm 1$) should produce a modulation of the spherical particle along the z axis. So, in principle the observed Raman band at 19.2 cm^{-1} could be attributed to such modes. However, the calculated frequency is found around 12.1 cm^{-1} (Table 1). This frequency is nearly 7 cm^{-1} smaller than the experimental value. Therefore, we assign the Raman signal from the NCls (Figures 3 and 5) to the SLM ($l = 2$, $m = \pm 2$) rather than to SLMs ($l = 2$, $m = 0, \pm 1$).

Moreover, the MD calculations show that, for aspect ratios $\boldsymbol{H}/\boldsymbol{D}_{NCl} > 2$, the frequency of SLM ($l = 2$, $m = \pm 2$) is rather constant (around $S = 0.8$). Indeed, for these modes, the prolate particle does not vibrate along its major axis and hence the vibrational frequencies do not depend on the particle height $\boldsymbol{H}$ in the limit $\boldsymbol{H}/\boldsymbol{D}_{NCl} >> 1$. Because the aspect ratio of the NCls is $\boldsymbol{H}/\boldsymbol{D}_{NCl} = 2.5 \pm 0.3$, shape fluctuations are not directly responsible for inhomogeneous broadening of the Raman band (Figures 3 and 5). However, taking into account the measured dispersion[17] in the NCl's diameter, $\boldsymbol{D}_{NCl_{min}} = 2.5$ nm and $\boldsymbol{D}_{NCl_{max}} = 2.9$ nm and using $S = 0.8$, one can easily estimate that the frequency of the SLMs ($l = 2$, $m = \pm 2$) falls in the range of 18.5−21 cm^{-1}. So, one expects a shift of the Raman band toward lower frequencies when decreasing the excitation wavelength due to selection of NCls with smaller aspect ratios (i.e., larger $\boldsymbol{D}_{NCl}$ values). Figure 4 shows instead a shift to higher frequencies. This indicates that the overall width and frequency of the Raman band cannot only be interpreted in terms of size/shape-induced inhomogenous broadening. The coupling mechanisms between the SPR and the NCl's vibrations as well as the dependence of the Raman efficiency on excitation wavelength need to be identified in order to fully account for the Raman data.

Collective effects among the NCls may also be important for the excitation step of the Raman scattering process because they could enhance the absorption of the incident photons.[38] However, because the mechanical coupling between the NCls and the matrix is rather weak in the present case, the acoustic vibrations are most likely localized within each NCl and there would not be spatial phase coherence between the vibration of a NCl and its neighbors. Therefore, the overall Raman process would be spatially incoherent and not affected by possible electromagnetic interactions between NCls, this being in agreement with recent results reported on self-ordered silver spherical nanoparticles.[38] As a consequence, low-frequency Raman scattering can be interpreted in this case in terms of individual scattering objects and inhomogeneous broadening effects, as opposed to what happens in the case of semiconductor quantum dots embedded in a semiconductor matrix where strong collective effects are observed.[39] Therefore, the vibrational coupling between nanoobjects and its effects on the plasmon-mediated resonant Raman scattering is one of the most interesting points, which needs further modeling of both vibrational and Plasmon modes in order to fully understand their interaction.

In summary, we have reported on the structural, optical, and vibrational properties of novel self-assembled silver NCls produced by alternate PLD. We have developed a new technique to produce NCls self-aligned along the growth direction with small size and shape dispersions. This allowed us to study the optical and vibrational properties as a function of NCl shape and to observe, for the first time in such self-assembled nanostructures, the splitting of the SPR into longitudinal and transverse modes. The comparison of the measured extinction spectra and those simulated using the simple model of Gans for embedded spheroids, and Maxwell−Garnett effective medium model suggests that electromagnetic interactions among NCls might play a role in the optical response. The resonant Raman scattering produced by confined acoustic vibrations of self-assembled NCls has also been reported for the first time, and the self-alignment of the NCls has allowed the investigation of Raman selection rules, the analysis of the scattering process in terms of optical excitation and detection, and the study of the interaction between surface plasmon and vibration modes. The vibrational frequencies of the twofold degenerate spheroidal-like modes ($l = 2$, $m = \pm 2$) calculated using molecular dynamics, and corrected for the matrix effect, agree very well with the measured Raman band frequencies. We have identified that the interaction between the longitudinal surface plasmon mode and the vibrational spheroidal-like mode ($l = 2$, $m = \pm 2$) activates the scattering acoustic Raman signal.

This work thus opens new routes for the understanding of surface plasmons and confined acoustic phonons in metal nanoobjects and their interaction mechanisms. However,

some fundamental questions remain open. For instance, how do acoustic vibrations of nano-objects depend on their size and shape? What is the characteristic distance below which the acoustic vibrations and SPR exhibit collective effects? How do acoustic vibrations inelastically scatter light via interaction with SPR?

Acknowledgment. This work was partially supported by MAT2005-06508-C02-01, MEC (Spain), and by EU Network HPRN-CT-2002-00328. J.M. acknowledges an I3P fellowship from the CSIC and the European Social Fund. D.B.M. acknowledges support from NSERC.

References

(1) Itoh, T.; Biju, V.; Ishikawa, M.; Kikkawa, Y.; Hashimoto, K.; Ikchov, A.; Ozaki, Y. *J. Chem. Phys.* **2006**, *124*, 134708.
(2) Laurent, G.; Félidj, N.; Aubard, J.; Lévi, G. *J. Chem. Phys.* **2005**, *122*, 011102.
(3) Jeong, D. H.; Zhang, Y. X.; Moskovits, M. *J. Phys. Chem. B* **2004**, *108*, 12724.
(4) Yao, J. L. *Pure Appl. Chem.* **2000**, *72*, 221.
(5) Johansson, P.; Xu, H.; Köll, M. *Phys. Rev. B* **2005**, *72*, 035427.
(6) De Marzi, G.; Iacopino, D.; Quinn, A. J.; Redmond, G. *J. Appl. Phys.* **2004**, *96*, 3458.
(7) Maier, S. A.; Brangesma, M. L.; Kik, P. G.; Atwater, H. A. *Phys. Rev. B* **2002**, *65*, 193408.
(8) Liu, X.; Luo, J.; Zhu, J. *Nano Lett.* **2006**, *6*, 408.
(9) Zielasek, V.; Block, T.; Pfnur, H. *Rev. Adv. Mater. Sci.* **2004**, *8*, 1.
(10) Borowiak-Palen, E.; Ruemmeli, M. H.; Gemming, T.; Pichler, T.; Kalenczuk, R. J.; Silva, S. R. P. *Nanotechnology* **2006**, *17*, 2415.
(11) Yang, C.; Wan, C.; Wang, Y. *J. Electrochem. Soc.* **2006**, *153*, J27.
(12) Xiong, Y. J.; Xie, Y.; Wu, C.; Yang, J.; Li, Z.; Xu, F. *Adv. Mater.* **2003**, *15*, 405.
(13) Li, C.; Yang, X.; Yang, B.; Yan, Y.; Qian, Y. *Mater. Lett.* **2005**, *59*, 1409.
(14) Sakamoto, Y.; Fukuoka, A.; Higuchi, T.; Shimomura, N.; Inagaki, S.; Ichikawa, M. *Phys. Chem. B* **2004**, *108*, 853.
(15) Zach, M. P.; Ng, K. H.; Penner, R. M. *Science* **2000**, *290*, 2120.
(16) Gonzalo, J.; Serna, R.; Solis, J.; Babonneau, D.; Afonso, C. N. *J. Phys.: Condens. Matter* **2003**, *15*, S3001.
(17) Margueritat, J.; Gonzalo, J.; Afonso, C. N.; Ortiz, M. I.; Ballesteros, C. *Appl. Phys. Lett.* **2006**, *88*, 093107.
(18) Hövel, H.; Fritz, S.; Hilger, A.; Kreibig, U. *Phys. Rev. B* **1993**, *48*, 24.
(19) Ditlbacher, H.; Krenn, J. R.; Lamprecht, B.; Leitner, A.; Aussenengg, F. R. *Opt. Lett.* **2000**, *25*, 563.
(20) Rechberger, W.; Hohenau, A.; Leitner, A.; Krenn, J. R.; Lamprecht, B.; Aussenegg, F. R. *Opt. Commun.* **2003**, *220*, 137.
(21) Sosa, I. O.; Noguez, C.; Barrera, R. G. *J. Phys. Chem. B* **2003**, *107*, 6269.
(22) Sweatlock, L. A.; Maier, S. A.; Atwater, H. A.; Penninkhof, J. J.; Polman, A. *Phys. Rev. B* **2005**, *71*, 235408.
(23) Link, S.; El-Sayed, M. A. *Int. Rev. Phys. Chem.* **2000**, *19*, 409.
(24) Coronado, E. A.; Schatz, G. C. *J. Chem. Phys.* **2003**, *119*, 3926.
(25) Serna, R.; De Sande, J. C.; Ballesteros, J. M.; Afonso, C. N. *J. Appl. Phys.* **1998**, *84*, 4509.
(26) Gans, R. *Ann. Phys.* **1925**, *76*, 29.
(27) Johnson, P. B.; Christy, R. W. *Phys. Rev. B* **1972**, *6*, 4370.
(28) Maxwell, Garnett, J. C. *Philos. Trans. R. Soc. London, Ser. A* **1904**, *203*, 385; **1906**, *205*, 237.
(29) Fujii, M.; Hayashi, S.; Yamamoto, K. *Phys. Rev. B* **1991**, *44*, 6243.
(30) Duval, E.; Portales, H.; Saviot, L.; Fujii, M.; Sumitomo, K.; Hayashi, S. *Phys. Rev. B* **2001**, *63*, 075405.
(31) Portales, H.; Saviot, L.; Duval, E.; Fujii, M.; Hayashi, S.; Del Fatti, N.; Vallée, F. *J. Chem. Phys.* **2001**, *115*, 3444.
(32) Bachelier, G.; Mlayah, A. *Phys. Rev. B* **2004**, *69*, 205408.
(33) Lamb, H. *Proc. London Math. Soc.* **1882**, *13*, 189.
(34) Del Fatti, N.; Voisin, C.; Chevy, F.; Vallée, F.; Flytzanis, C. *J. Chem. Phys.* **1999**, *110*, 11484.
(35) Palpant, B.; Portales, H.; Saviot, L.; Lerme, J.; Prevel, B.; Pellarin, M.; Duval, E.; Perez, A.; Broyer, M. *Phys. Rev. B* **1999**, *60*, 17107.
(36) Chronological Scientific Tables, Maruzen, Tokyo, 1991.
(37) Saviot, L.; Murray, D. B.; Marco de Lucas, M. C. *Phys. Rev. B* **2004**, *69*, 113402.
(38) Duval, E.; Mermet, A.; Courty, A.; Albouy, P. A.; Pileni, M. P. *Phys. Rev. B* **2005**, *72*, 085439.
(39) Cazayous, M.; Groenen, J.; Huntzinger, J. R.; Mlayah, A. *Phys. Rev. B* **2001**, *64*, 033306.

NL061237H